

Combinatorial screening of cell proliferation on poly(L-lactic acid)/poly(D,L-lactic acid) blends [☆]

Carl G. Simon Jr.^{a,*}, Naomi Eidelman^b, Scott B. Kennedy^{a,1}, Amit Sehgal^{a,2},
Chetan A. Khatri^{a,3}, Newell R. Washburn^{a,4}

^aPolymers Division, National Institute of Standards and Technology, 100 Bureau Drive, Gaithersburg, MD 20899-8545, USA

^bPaffenbarger Research Center, American Dental Association Foundation, National Institute of Standards and Technology, Gaithersburg, MD 20899, USA

Received 21 January 2005; accepted 17 April 2005
Available online 6 June 2005

Abstract

We have combined automated fluorescence microscopy with a combinatorial approach for creating polymer blend gradients to yield a rapid screening method for characterizing cell proliferation on polymer blends. A gradient in polymer blend composition of poly(L-lactic acid) (PLLA) and poly(D,L-lactic acid) (PDLLA) was created in the form of a strip-shaped film and was annealed to allow PLLA to crystallize. Fourier transform infrared (FTIR) microspectroscopy was used to determine the composition in the gradients and atomic force microscopy was used to characterize surface topography. Osteoblasts were cultured on the gradients and proliferation was assessed by automated counting of cells using fluorescence microscopy. Surface roughness varied with composition, was smooth on PDLLA-rich regions and was rough on the PLLA-rich regions. Cell adhesion was similar on all regions of the gradients while proliferation was faster on the smooth, PDLLA-rich end of the gradients than on the rough, PLLA-rich end of the gradients. These results demonstrate the feasibility of a new, combinatorial approach for evaluating cell proliferation on polymer blends.

Published by Elsevier Ltd.

Keywords: Combinatorial methods; Polymer blends; Cell proliferation; Polylactic acid; Microspectroscopic FTIR; Osteoblast

1. Introduction

Polymer blending is a common and inexpensive method to create new materials with desirable properties and nearly one quarter of manufactured polymers are

used in blends [1,2]. Polymer blending can be used to optimize material properties such as modulus, strength, morphology, crystallinity and biocompatibility, and, in turn, these properties can affect cell response [3–5]. In order to advance the ability of tissue engineers to study cell response to polymer blends, we have combined automated fluorescence microscopy with a combinatorial approach for creating polymer blend gradients to yield a rapid method for characterizing cell proliferation on polymer blends.

Current methods for the development of biomaterials require preparing and characterizing individual materials one at a time. Although this approach is effective, it can be costly and time-consuming. Conversely, the application of combinatorial and high-throughput methods to materials design could potentially accelerate

[☆]This article, a contribution of National Institute of Standards and Technology, is not subject to US copyright.

*Corresponding author. Tel.: +301 975 8574; fax: +301 975 4977.

E-mail address: carl.simon@nist.gov (C.G. Simon Jr.).

¹New Address: Department of Chemistry, Eastern Mennonite University, Harrisonburg, VA 22802-2462, USA.

²New Address: Complex Fluids Lab, Rhodia, Inc., Cranbury, NJ 08512-7500, USA.

³New Address: Biosurgical Research and Development, Ethicon, Inc., Somerville, NJ 08876, USA.

⁴New Address: Departments of Chemistry and Biomedical Engineering, Carnegie Mellon University, Pittsburgh, PA 15213, USA.

research in this field [6]. Towards this end, several groups have devised combinatorial and high-throughput methods for biomaterials development [7–11]. In the current study, we present a new, combinatorial method for examining cell proliferation on polymer blends.

A three-syringe pump system with a mixing vial was used to create a gradient in polymer composition of two polymers along the barrel of syringe. The gradient was deposited from the syringe onto a substrate using a motorized stage to yield a two-dimensional composition gradient in the form of a strip-shaped film [4,12]. Gradients were made from two polymers commonly used in biomaterials, poly(L-lactic acid) (PLLA) and poly(D,L-lactic acid) (PDLLA). PLLA and PDLLA are chemically similar and differ only in their tacticity such that PLLA is crystalline and PDLLA is amorphous. PLLA also has a higher modulus than PDLLA [10,13]. The composition of the gradients was determined by Fourier transform infrared (FTIR) microspectroscopy and cells were cultured on the gradient films. Cell adhesion and proliferation were analyzed with automated fluorescence microscopy. The results show that cell proliferation was enhanced on PDLLA-rich regions of the gradients and demonstrate the feasibility of this unique combination of composition gradient technology and automated fluorescence microscopy.

2. Materials and methods

2.1. Preparation of polymer films

Polymer composition gradients were prepared from PLLA ($M_w = 300,000$; Polysciences, Warrington, PA) and PDLLA ($M_w = 330,000$ – $600,000$; Polysciences, Warrington, PA) as described elsewhere [4,10,12]. Briefly, a solution of PDLLA was infused from a syringe at a rate of 1 mL/min into a mixing vial containing 2 mL of PLLA (with stir bar) while a second syringe removed the polymer mixture at a rate of 2 mL/min. Meanwhile, a third syringe sampled the mixing vial by withdrawing 0.075 mL of blended polymer solution over 2 min to yield a composition gradient in the barrel of this third 'sampling' syringe. The gradient was deposited from the sampling syringe onto a Low-e slide (Kevley Technologies, Chesterland, OH) using a motorized stage and the bead of polymer solution was allowed to dry into a strip-shaped film [10] that was approximately 4 μm thick as determined by profilometry (Dektak 8 Stylus Profilometer, Veeco, Woodbury, NY). Low-e microscope slides have a coating which reflects the infrared light back through the polymer film to yield reflection-transmission spectra [14].

Twelve composition gradients were prepared that were approximately 50 \times 4 mm. Control strip films of five discrete blend compositions (0%, 25%, 50%, 75%, 100% mass fraction PLLA) were also prepared for FTIR calibration. All of the gradient and control films were melted at 200 °C for 5 min (above T_m) and then annealed at 120 °C for 8 h (between T_g and T_m) under nitrogen to remove residual solvent and to

induce crystallization of the PLLA. Surface topography of the films was examined with tapping-mode atomic force microscopy (AFM) using a Dimension 3100 Nanoscope IIIa (Veeco Instruments, Inc., Woodbury, NY). Birefringence from spherulites was observed in a transmitted-light microscope using crossed polarizers.

2.2. FTIR microspectroscopy

FTIR reflection-transmission microspectroscopy (FTIR-RTM) [14] was utilized to map six of the PLLA-PDLLA gradients and the five calibration control films. A Nicolet Magna-IR 550 FTIR spectrophotometer (Madison, WI) interfaced with a Nic-Plan IR microscope with an automated stage (Spectra-Tech, Inc., Shelton, CT, USA) and the Atlas mapping software (Thermo Electron Corp., Madison, WI) was used. Matrices of spectra (1872–2310 spectra per map) were collected from 4000 to 650 cm^{-1} (spectral resolution 8 cm^{-1} , 32 scans per spectrum, spot size 0.2 \times 0.2 mm). The 1270 cm^{-1} peak (ester C–O stretch) [15] is dependent on PDLLA concentration and the 1450 cm^{-1} peak (methyl asymmetrical bending) [15] is constant and serves as an internal standard [14]. The map in Fig. 2b was processed as ratios between the areas of the 1270 cm^{-1} and the 1450 cm^{-1} peaks [(1246–1286) cm^{-1} and (1420–1500) cm^{-1} spectral regions, respectively] and presented as a color contour map. The color thresholds for this map were adjusted manually to achieve optimal color contrast between the ends of the gradient.

For quantitative determination of the compositions of the gradients (Fig. 2c), the maps of the control discrete blends and maps of the gradients were imported into the ISys software package (Spectral Dimensions Inc., Olney, MD). The ratios between the 1270 cm^{-1} and the 1450 cm^{-1} peaks were calculated for all spectra in the same spectral regions used in processing the color contour maps. A calibration curve (linear regression, $R^2 = 0.998$) was constructed from the discrete blend strip films [(25, 50, 75 and 100) % PLLA] by plotting the ratios of the 1270 cm^{-1} peak and the 1450 cm^{-1} peak versus the fraction of PLLA in each discrete film. This calibration curve was used to determine the composition of the gradients as previously described [14].

2.3. Cell culture

MC3T3-E1 cells are a well-characterized murine osteoblast-like cell line which serve as a model for endogenous osteoblasts [16]. Established protocols for the culture and passage of MC3T3-E1 cells were followed [17]. Cells were obtained from Riken Cell Bank (Hirosaka, Japan) and cultured in flasks (75 cm^2 surface area) at 37 °C in a fully humidified atmosphere at 5% CO_2 (volume fraction) in alpha-modification of Eagle's minimum essential medium (Cambrex Bio Science, Walkersville, MD) supplemented with 10% volume fraction fetal bovine serum (Gibco, Rockville, MD) and 0.060 mg/mL kanamycin sulfate (Sigma, Inc., St. Louis, MO). Medium was changed twice weekly and cultures were passaged with 2.5 g/L trypsin (0.25% mass fraction) containing 1 mmol/L EDTA (Gibco, Rockville, MD) once per week. Cultures of 80% confluent MC3T3-E1 cells were used for all experiments.

The 12 PLLA-PDLLA gradients were sterilized in 70% ethanol (mass fraction) for 5 min, rinsed in media and seeded with 10^6 MC3T3-E1 cells in 150 cm² petri dishes (7000 cells/cm²) with 50 mL of media. Six plain glass slides were also sterilized and seeded with cells as controls. Gradients and controls were incubated with cells for 4 d, fixed for 5 min (0.5% mass fraction Triton X-100, 4% mass fraction paraformaldehyde, 5% mass fraction sucrose, 1 mmol/L CaCl₂, 2 mmol/L MgCl₂ in phosphate buffered saline, pH 7.4) and post-fixed for 20 min (same as fix but without Triton X-100). Fixed cells were fluorescently stained for 1 h with 6 μmol/L 4',6-diamidino-2-phenylindole, dihydrochloride (DAPI) and 2 μmol/L Texas Red C₂-maleimide (both from Molecular Probes, Eugene, OR) in phosphate-buffered saline. DAPI stains cell nuclei blue and Texas Red C₂-maleimide stains cell membranes red [18]. Stained cells were mounted with a coverslip in Vectashield containing DAPI (Vector Laboratories, Inc., Burlingame, CA).

2.4. Automated fluorescence microscopy

The number of cells present on the gradients was quantified by counting DAPI-stained cell nuclei using automated fluorescence microscopy with a Leica DMR 1200 upright microscope equipped with a computer-controlled translation stage (Vashaw Scientific, Inc., Frederick, MD). Image Pro software (Media Cybernetics, Carlsbad, CA) was used to run the stage and image acquisition. A 50 × 3 matrix of images was taken of each composition gradient and of each glass control slide using automated microscopy. Images were acquired with a 10 × eyepiece and a 10 × objective (100 × magnification) and approximately 25% of the surface of each gradient was imaged. The number of nuclei present in each of the images was tabulated using a macro that was written for Image Pro. The macro opens each image file, counts the number of nuclei and records the number in a text file. The text files were imported into Microsoft Excel and analyzed. Images of cell morphology were acquired manually using the same equipment described above but through a red fluorescence filter cube to image Texas Red C₂-maleimide-stained cell membranes.

2.5. Statistics

When a 'standard deviation' is given in the text or shown as an error bar on a plot, it refers to the 'standard deviation of the mean', which is the same as the 'combined standard uncertainty of the mean' for the purposes of this work. ANOVA with Tukey's test for multiple comparisons was used to analyze the cell adhesion and proliferation data.

2.6. Note

Certain equipment and instruments or materials are identified in the paper to adequately specify the experimental details. Such identification does not imply recommendation by the National Institute of Standards and Technology, nor does it imply the materials are necessarily the best available for the purpose.

3. Results

Control films of pure PDLLA and pure PLLA were melted and annealed as a reference for the gradients. Control films of pure PDLLA did not contain birefringent spherulites when viewed with crossed polarizers (Fig. 1a) and they had a smooth surface topography (RMS roughness = 4 nm; Fig. 1b). In contrast, control films of pure PLLA contained birefringent spherulites (Fig. 1c) and had a coarse surface topography (RMS roughness = 43 nm; Fig. 1d) that was ten times rougher than PDLLA. Unannealed PLLA films were similar to PDLLA films in that they did not contain spherulites, were not birefringent and had a smooth surface topography (data not shown).

Twelve PLLA-PDLLA composition gradients were prepared and FTIR-RTM [14] was used to characterize six of them. The color contour map of one of the gradients is shown in Fig. 2b. Blue indicates PDLLA-rich regions of the gradients and orange represents PLLA-rich regions. The map shows that a qualitative gradient in composition was present in the film and similar trends were found in the other five gradient films that were mapped. A plot of averaged quantitative composition data taken from the spectra of the six gradients that were mapped is shown in Fig. 2c. Linear regression was used to fit the solid line to the data in Fig. 2c and shows that the composition gradients in the films are nearly linear ($R^2 = 0.94$). There are also some compositional fluctuations in the gradients. For example, the compositions at 0 and 10 mm are similar and the gradient is nearly flat from 35 to 45 mm. The equation

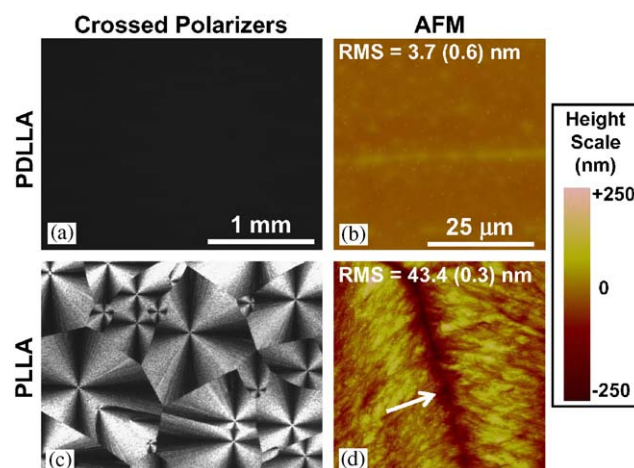


Fig. 1. Control films of pure PLLA and pure PDLLA were melted and annealed. (a) PDLLA through crossed polarizers. (b) PDLLA in AFM. (c) PLLA through crossed polarizers. (d) PLLA in AFM. The size bar in (a) also applies to (c) and the size bar in (b) also applies to (d). RMS roughness (root mean square) was measured three times on three film specimens for each polymer and averages with S.D. of the mean are given in (b) and (d). The arrow in (d) points to a grain boundary between two spherulites and a height scale for the AFM images is given on the far right of the figure.

describing the linear fit in Fig. 2c was used to translate “Position” along the gradients into “Fraction PLLA” along the gradients. The average error on the composition values in Fig. 2c was 5.0% (average height of the y -error bars) which implies that composition values throughout the manuscript have an approximate error of $\pm 5\%$. These data show that gradients in polymer composition existed in the films and that the gradients ran from 25% to 100% PLLA.

Transmitted light microscopy through crossed polarizers was also used to characterize the composition gradients. In Fig. 2a, a composite of 46 overlapping images taken of a gradient was assembled and shows that birefringence changes with composition. Increased PLLA content corresponded to increased birefringence since PLLA is crystalline and PDLLA is amorphous. Similar gradients in birefringence existed in all 12 composition gradients that were made. Higher magnification images showed that spherulite morphology also varied with composition (data not shown). PDLLA-rich

ends of the gradients were completely amorphous and did not contain any birefringent spherulites while PLLA-rich ends of the gradients contained only spherulites and no amorphous regions. Middle regions of the gradients had areas where part of the volume was spherulitic and part of the volume was amorphous. This resulted in regions where a lone spherulite might be surrounded by amorphous polymer, or an amorphous zone might be surrounded by a number of spherulites. These morphologies were observed in discrete PLLA-PDLLA blends in earlier studies [19], PLLA-PDLLA gradients in a previous study [10] and in the FTIR calibration films of the present work (data not shown). Gradients in birefringence and spherulite morphology were present in all 12 gradients that were made. These data serve as an additional indicator that our specimens contained gradients in polymer composition.

AFM (Fig. 3) revealed that surface roughness varied across the gradients, was dependent on composition but was not predictive of composition. Spherulites having a

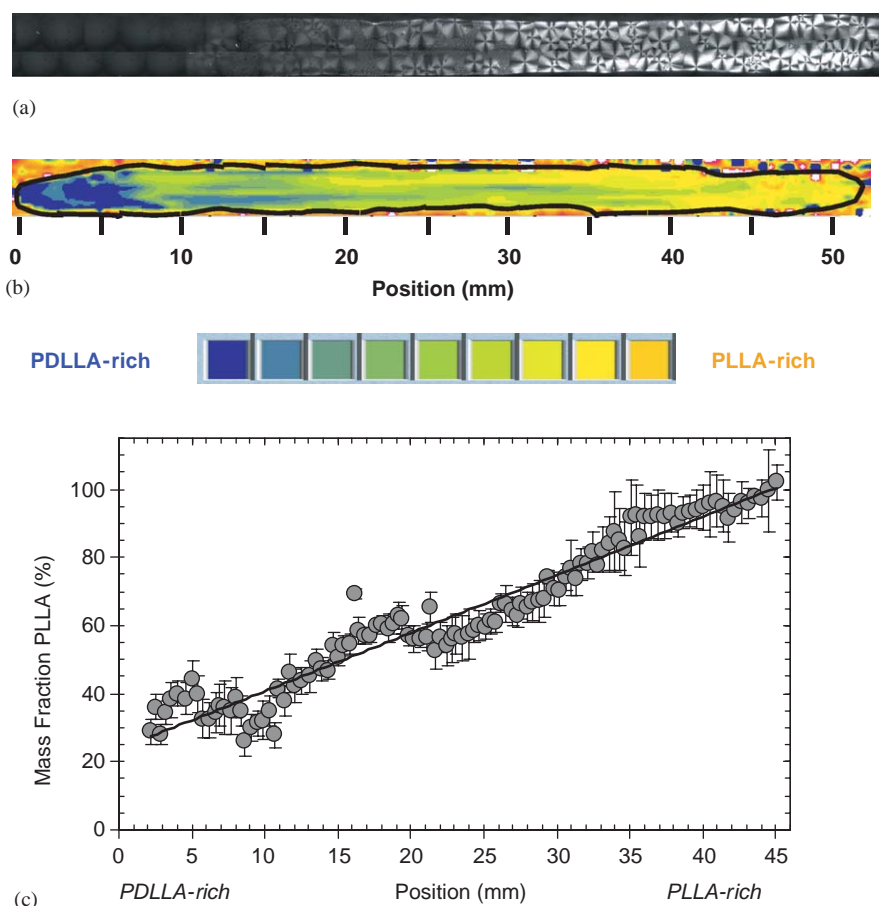


Fig. 2. (a) An image of the birefringence from a PLLA-PDLLA gradient is shown. Forty-six overlapping images taken through crossed polarizers using transmitted light microscopy were assembled into the final image shown. The higher crystallinity of the PLLA-rich end of the gradient causes it to be more birefringent than the PDLLA-rich end. The gradient shown is 52 mm long. (b) FTIR-RTM map of a PLLA-PDLLA composition gradient. The strip film has been outlined with a black line. A qualitative gradient in color is visible in the film, with blue corresponding to PDLLA-rich regions and orange corresponding to PLLA-rich regions (see color bar below map). Pixels located outside the black borders represent artefacts from bare regions on the slides and were not included in the composition calculations. (c) The compositions of six PLLA-PDLLA gradients determined with FTIR-RTM were averaged and plotted versus position.

roughness similar to pure PLLA (Fig. 1d) formed on the PLLA-rich ends of the gradients (Fig. 3f–g) while the PDLLA-rich ends were smooth and amorphous (Fig. 3a) similar to pure PDLLA (Fig. 1b). Starting from the PDLLA-rich end, surface RMS roughness of the gradients increased as the fraction of PLLA increased (Fig. 3(h)). Roughness then reached a plateau between 60% to 80% PLLA (Fig. 3(h)) before becoming somewhat smoother from 80% to 100% PLLA. Although there is not a well-defined correlation between blend composition and surface roughness, these results show that surface topography varied across the gradients.

Osteoblast-like MC3T3-E1 cells [16] were cultured on the gradients and on control glass slides for 1 or 4 d and

then cell morphology was examined by fluorescence microscopy. After 1 d, cells were spindly on all regions of the gradients (Fig. 4a and b) but were well spread on glass (Fig. 4c). By 4 d, cells were well spread and attained a normal, polygonal morphology on the PLLA-PDLLA gradients and on the glass controls (Fig. 4d–f).

Cell adhesion and proliferation were examined by counting cells per mm^2 using automated fluorescence microscopy (Fig. 5). Adhesion at 1 d was similar on all regions of the gradients (open circles, Fig. 5b) but proliferation by 4 d was faster on the PDLLA-rich ends of the gradients (closed circles, Fig. 5b). Proliferation was fastest at 25–35% PLLA but was slower and nearly monotonic on the rest of the compositions (35–100%

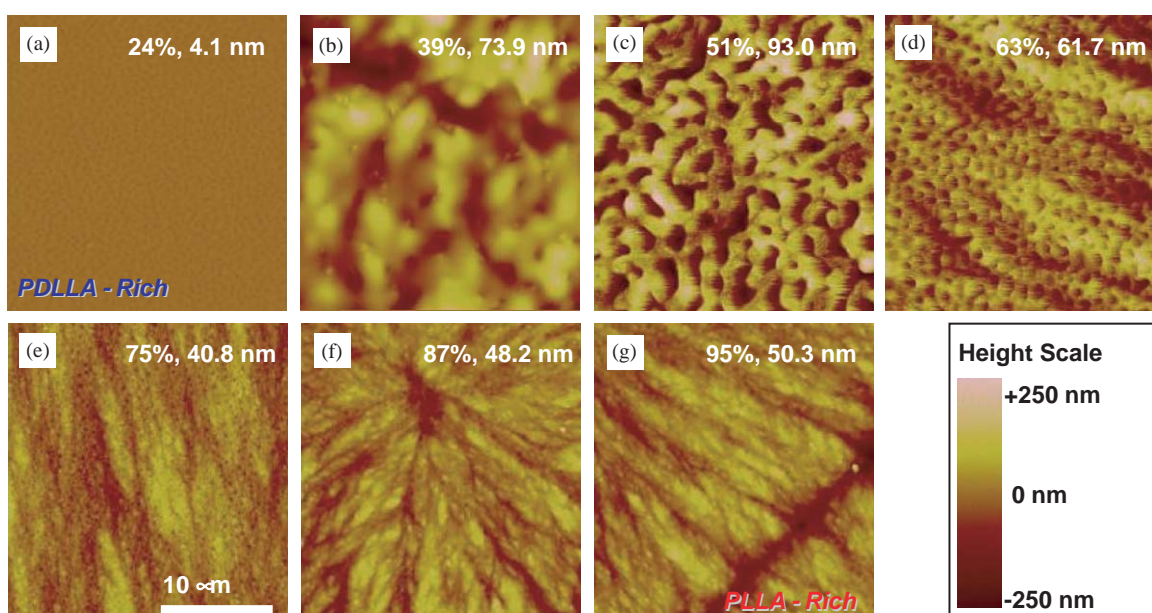


Fig. 3. Surface topography of the gradients varies with composition. (a–g) AFM height images taken from a PLLA-PDLLA gradient are shown. Mass fraction PLLA (calculated from linear regression in Fig. 2c) and RMS roughness is given at the top of each image. The height scale for all the images is provided to the right of (g). (h) The RMS roughness data from six gradients was averaged and plotted against composition. Note that x-error bars of 5.0% have been omitted for clarity.

PLLA). As a control, cell numbers across glass slides were determined at 1 and 4 d (Fig. 5a). As expected, cell adhesion at 1 d (open circles) and proliferation at 4 d (closed circles) were not affected by position on the glass slides.

The cell number data was analyzed by ANOVA with Tukey's test for multiple comparisons to determine significant differences using Sigmaplot software (Systat Software, Inc., Point Richmond, CA). In order to make the data analysis manageable, the data points from each of the four plots in Fig. 5 were grouped into sets of 3, re-averaged and re-plotted in Fig. 6a–d. Each data point for a particular plot (a–d) was compared to each of the other points in that plot to test for significant differences. Significant differences ($p < 0.05$) are indicated by grey shading in the tables to the right of each of the plots in Fig. 6. Predictably, there are no shaded boxes in the tables to the right of Fig. 6a–b which indicates that there were no positions on the control glass slides where cell adhesion (Fig. 6a) or proliferation (Fig. 6b) were significantly different from that of other positions on the glass slides. There are some significant differences in cell adhesion on the gradients after 1 d (Fig. 6c) but these differences are inconsistent. However, after 4 d on the gradients (Fig. 6d) cell number at 29% PLLA (mass fraction) was significantly different from the other positions on the gradient. These data indicate that cell proliferation was enhanced on the PDLLA-rich end of the gradients.

In Fig. 6e, data from “gradients, 4 d” was further analyzed by plotting the cell number data against surface roughness. These data were also binned and statistically analyzed as described above. The data show that cell proliferation was significantly faster on the smoothest portions of the gradients (RMS roughness of 11 nm) than on the rougher portions of the gradients

(RMS roughness between 17 and 70 nm). These results seem to suggest that cell proliferation is enhanced by the smoother surface topography of the PDLLA-rich blends. However, it is not possible to distinguish if the cause of the enhanced proliferation is a result of composition or surface roughness since both parameters vary across the gradients.

4. Discussion

Several previous studies have examined cell behavior on PLLA and PDLLA and the general conclusion from these efforts is that cells can adhere, proliferate and differentiate on these polymers [20–27]. Three studies directly compared cell response to PLLA and PDLLA [20,21,24]. Ishaug-Riley et al. [24] found that human chondrocyte adhesion (8 h) and proliferation (7 d) are better on PLLA than on PDLLA. In contrast, van Sliedregt et al. [20,21] observed that several cell types (epithelial cells, fibroblasts and osteosarcoma cells) proliferate faster on PDLLA than on PLLA, obtain a normal morphology on both polymers but are unable to form a confluent monolayer on either polymer after 14 d culture. However, none of these studies used annealed polymers, which implies that their PLLA specimens did not have a spherulite-roughened surface topography as is seen herein with annealed PLLA.

Interestingly, effects of PLLA crystallinity on cell response have been reported [5,28,29]. Hepatocyte adhesion, proliferation and differentiation are enhanced on amorphous PLLA (un-annealed) as compared to crystalline PLLA (annealed) [29]. In addition, fibroblasts [29] and osteoblasts [5] were found to proliferate more quickly on amorphous PLLA (un-annealed) than on crystalline PLLA (annealed) and animal studies

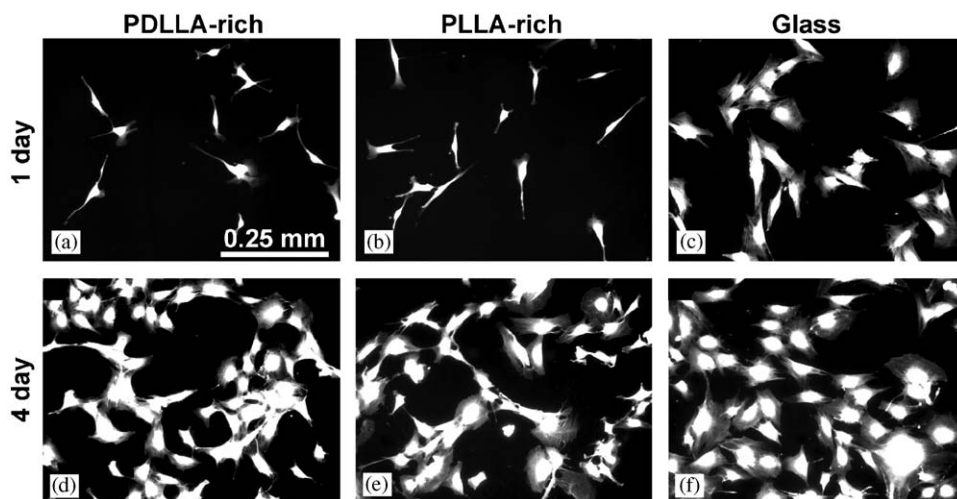


Fig. 4. Cell morphology on the PLLA-PDLLA gradients. Cells were imaged through a red fluorescent filter for the membrane stain, Texas Red C₂-maleimide: (a) 1 d, PDLLA-rich; (b) 1 d, PLLA-rich; (c) 1 d, glass; (d) 4 d, PDLLA-rich; (e) 4 d, PLLA-rich; (f) 4 d, glass. The size bar at the bottom of (a) is 0.25 mm and applies to all six images.

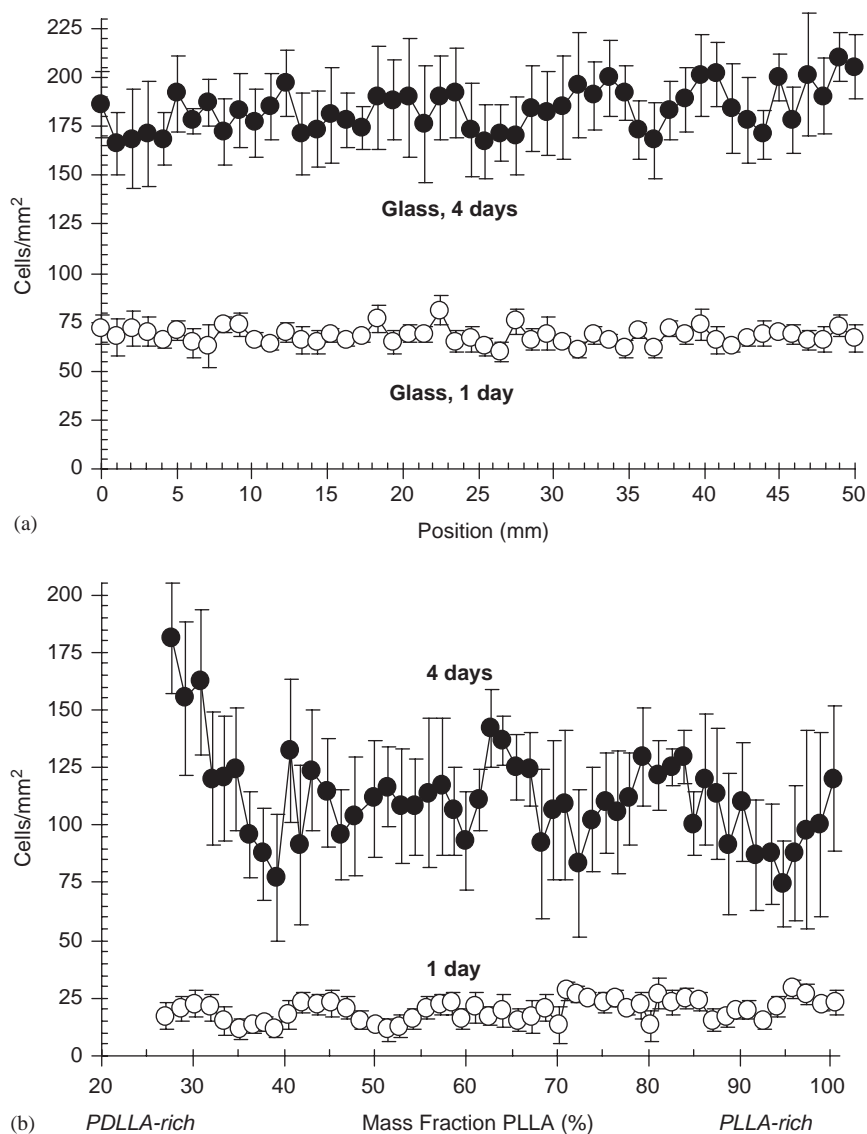


Fig. 5. Cell adhesion and proliferation on the PLLA-PDLLA gradients and on control glass slides was determined by using automated fluorescence microscopy to count cells. Images were taken through a blue fluorescence filter to count DAPI-stained cell nuclei. (a) The data from six glass slides for adhesion (1 d) and six glass slides for proliferation (4 d) were averaged and plotted against position on the slide. (b) The data from six gradients for adhesion (1 d) and six gradients for proliferation (4 d) were averaged and plotted against composition.

showed that tissue ingrowth is faster into amorphous PLLA scaffolds (un-annealed) than into crystalline PLLA scaffolds (annealed) [28]. In the current study, a similar trend of enhanced proliferation on amorphous poly lactides (i.e. the PDLLA-rich ends of annealed PLLA-PDLLA gradients) was observed (Fig. 5a and Fig. 6d).

It is well known that microscale surface topography can influence cell behavior [30] and this tenet seems to hold true for surface topography on the nanometric scale as well [4,5,30–33]. In addition, it is becoming clear that adsorbed proteins *in vitro* [18,34] and basement membranes *in vivo* [35,36] present a complex topography for cell adhesion and that this topography consists primarily of ridges, pores and fibers in the size range of

5–200 nm. In the current study, cells were cultured on PLLA-PDLLA composition gradients that contained regions of varied RMS roughness ranging from 8 to 80 nm. Cell proliferation was enhanced on the smooth regions of the gradients, but the results do not indicate whether the enhanced proliferation is caused by surface roughness or blend composition.

A number of high-throughput methods have emerged for characterizing cell response to variations in the properties of biomaterials. The material parameters that have been examined from a high-throughput perspective include surface energy [37], crystallinity [5], ligand-density [38–41] and composition [4,42–44]. In addition, a number of gradient [45,46] and discrete [47,48] techniques for high-throughput characterization of

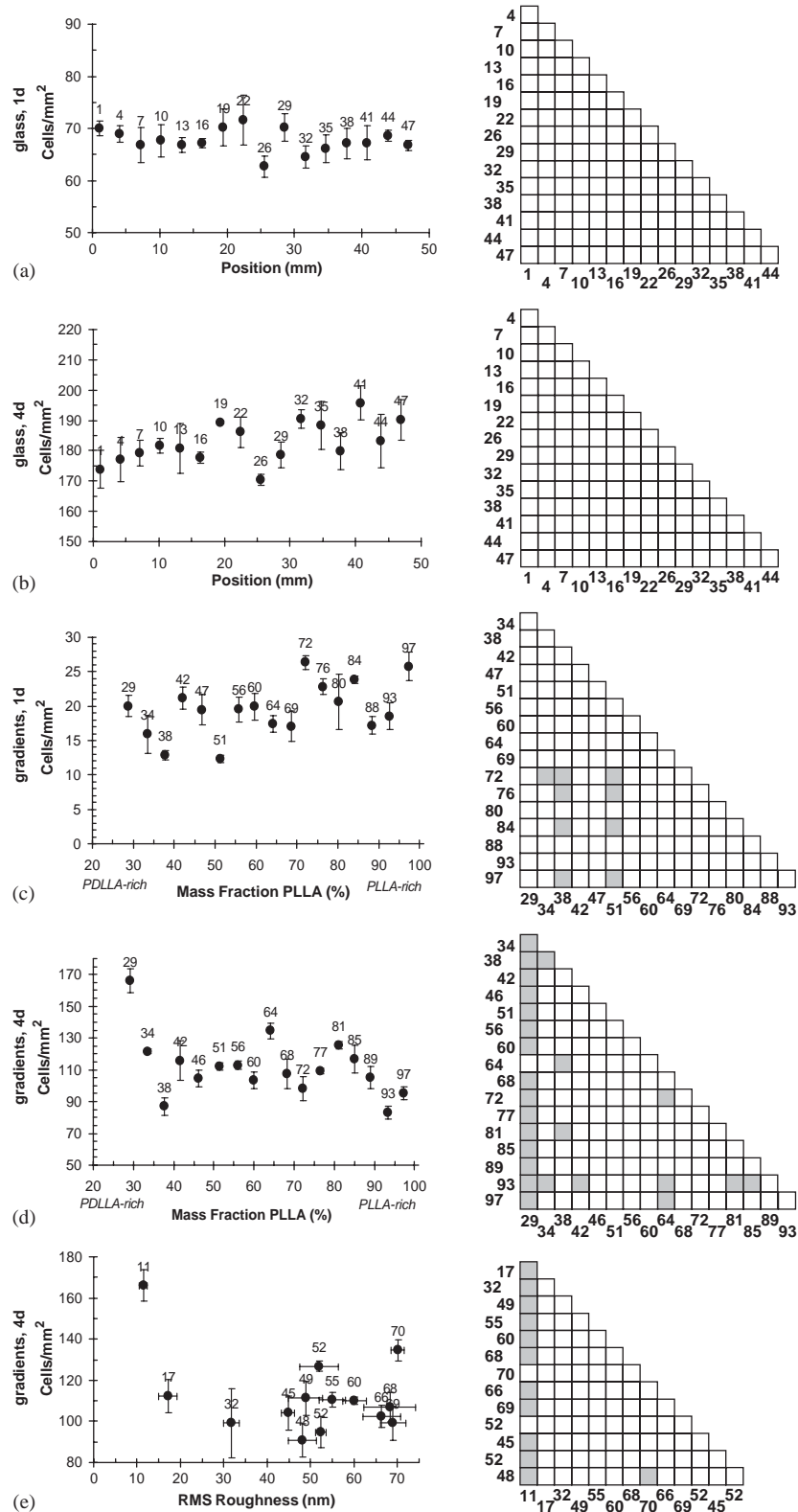


Fig. 6. A statistical analysis of the cell adhesion and proliferation data in Fig. 5 was performed using ANOVA with Tukey’s test for multiple comparisons. In order to make the analysis manageable, the number of data points from Fig. 5 was reduced by a binning process. Data points were grouped into sets of three, re-averaged and re-plotted: (a) glass, 1 d; (b) glass, 4 d; (c) gradients, 1 d; (d) gradients, 4 d. In (e), data from “gradients, 4 d” was further analyzed by plotting the cell number data against surface roughness. These data were also binned and statistically analyzed. Each data point for a particular plot (a–e) was compared to each of the other points in that plot to test for significant differences. Significant differences ($p < 0.05$) are indicated by gray shading in the tables to the right of each of the 5 plots. When x-error bars are not visible in the plots, they were smaller than the diameter of the data points. The x-values of the data points in the plots are shown above each point and are used to label the rows and columns in the tables to the right of the plots.

blends have also emerged. However, the novel combination of automated fluorescence microscopy and polymer composition gradient technology presented here is the only method optimized for rapidly screening cell proliferation on polymer blends.

5. Conclusions

A rapid method for screening cell proliferation on polymer blends was developed. Strip-shaped films containing a gradient in polymer composition were prepared and characterized with FTIR-RTM and AFM. Cells were cultured on the films and adhesion and proliferation were assessed using high-throughput, automated microscopy. Adhesion was similar on all regions of the gradients after 1 d but after 5 d proliferation was enhanced on the PDLLA-rich ends of the gradients. The PDLLA-rich ends of the gradients had smoother surface roughness than other regions on the gradients. The enhanced cell proliferation on PDLLA-rich regions of the gradients correlated with this smooth topography but it is unclear whether this is a result of blend composition or surface roughness since both parameters are varied across the gradients. These results suggest that, for the case of PLLA-PDLLA blends, PDLLA-rich blends that have a smooth surface are best-suited for supporting cell proliferation. In addition, these results demonstrate the feasibility of a new, combinatorial approach for evaluating cell proliferation on polymer blends.

Acknowledgments

We thank Wenhua Zhang for programming the computer-controlled translation stage and Sheng Lin-Gibson (NIST) and William F. Guthrie (NIST) for insightful discussions. This work was supported by NIH Y1-DE-1021, NIST and ADAF.

References

- [1] Paul DR. Polymer blends: phase behavior and property relationships. In: Paul DR, Sperling LH, editors. *Advances in chemistry series 211. Multicomponent polymer materials*. Washington, DC: American Chemical Society; 1986. p. 3–19.
- [2] Utracki LA. Processing two phase polymer systems. In: Utracki LA, editor. *Two-phase polymer systems*. New York: Hanser Publishers; 1991. p. 2.
- [3] Calvert JW, Marra KG, Cook L, Kumta PN, DiMilla PA, Weiss LE. Characterization of osteoblast-like behavior of cultured bone marrow stromal cells on various polymer surfaces. *J Biomed Mater Res* 2000;52:279–84.
- [4] Meredith JC, Sormana J-L, Keselowsky BG, Garcia AJ, Tona A, Karim A, Amis EJ. Combinatorial characterization of cell interactions with polymer surfaces. *J Biomed Mater Res* 2003;66A:483–90.
- [5] Washburn NR, Yamada KM, Simon Jr CG, Kennedy SB, Amis EJ. High-throughput investigation of osteoblast response to crystalline polymers: influence of nanometer-scale roughness on proliferation. *Biomaterials* 2003;25:1215–24.
- [6] Amis EJ. Combinatorial materials science: reaching beyond discovery. *Nature Mater* 2004;3:83–5.
- [7] Brocchini S, James K, Tangpasuthadol V, Kohn J. A combinatorial approach for polymer design. *J Am Chem Soc* 1997;119:4553–4.
- [8] Hoogenboom R, Meier MAR, Schubert US. Combinatorial methods, automated synthesis and high-throughput screening in polymer research: past and present. *Macromol Rapid Commun* 2003;24:15–32.
- [9] Anderson DG, Levenberg S, Langer R. Nanoliter-scale synthesis of arrayed biomaterials and application to human embryonic stem cells. *Nature Biotechnol* 2004;22:863–6.
- [10] Simon Jr CG, Eidelman N, Deng Y, Washburn NR. High-throughput method for determining modulus of polymer blends. *Macromol Rapid Commun* 2004;25:2003–7.
- [11] Smith JR, Seyda A, Weber N, Knight D, Abramson S, Kohn J. Integration of combinatorial synthesis, rapid screening, and computational modeling in biomaterials development. *Macromol Rapid Commun* 2004;25:127–40.
- [12] Meredith JC, Karim A, Amis EJ. High-throughput measurement of polymer blend phase behavior. *Macromolecules* 2000;33:5760–2.
- [13] Engelberg I, Kohn J. Physico-mechanical properties of degradable polymers used in medical applications: a comparative study. *Biomaterials* 1991;12:292–304.
- [14] Eidelman N, Simon Jr CG. Characterization of combinatorial polymer blend composition gradients by FTIR microspectroscopy. *J Res Natl Inst Stan* 2004;109:219–31.
- [15] Silverstein RM, Bassler GC, Morrill TC. *Spectrometric identification of organic compounds*, 4th ed. New York: Wiley; 1981. p. 106,123.
- [16] Sudo H, Kodama H-A, Magai Y, Yamamoto S, Kasai S. In vitro differentiation and calcification in a new clonal osteogenic cell line derived from newborn mouse calvaria. *J Cell Biol* 1983;96:191–8.
- [17] Simon Jr CG, Wight SA, Khatri CA, Wang FW. Preliminary report on the biocompatibility of a moldable, resorbable, composite bone graft consisting of calcium phosphate cement and poly(lactide-co-glycolide) microspheres. *J Orthopaed Res* 2002;20:473–82.
- [18] Elliott JT, Tona A, Woodward JT, Jones PL, Plant AL. Thin films of collagen affect smooth muscle cell morphology. *Langmuir* 2003;19:1506–14.
- [19] Tsuji H, Ikada Y. Blends of isotactic and atactic poly(lactide). 1. Effects of mixing-ratio of isomers on crystallization of blends from melt. *J Appl Polym Sci* 1995;58:1793–802.
- [20] van Sliedregt A, Radder AM, de Groot K, van Blitterswijk CA. In vitro biocompatibility testing of polylactides, Part I: Proliferation of different cell types. *J Mater Sci: Mater Med* 1992;3:365–70.
- [21] van Sliedregt A, de Groot K, van Blitterswijk CA. In vitro biocompatibility testing of polylactides, Part II: Morphologic aspects of different cell types. *J Mater Sci: Mater Med* 1993;4:213–8.
- [22] Ishaug SL, Yaszemski MJ, Bizios R, Mikos AG. Osteoblast function on synthetic biodegradable polymers. *J Biomed Mater Res* 1994;28:1445–53.
- [23] Göpferich A, Peter SJ, Lucke A, Lu L, Mikos AG. Modulation of marrow stromal cell function using poly(D,L-lactic acid)-block-poly(ethylene glycol) monomethyl ether surfaces. *J Biomed Mater Res* 1999;46:390–8.
- [24] Ishaug-Riley SL, Okun LE, Prado G, Applegate MA, Ratcliffe A. Human articular chondrocytes adhesion and proliferation on

- synthetic biodegradable polymer films. *Biomaterials* 1999;20:2245–56.
- [25] Ikarashi Y, Tsuchiya T, Kaniwa M-A, Nakamura A. Activation of osteoblast-like MC3T3-E1 cell responses by poly(lactide). *Biol Pharm Bull* 2000;23:1470–6.
- [26] Suh H, Hwang Y-S, Lee JE, Han CD, Park J-C. Behavior of osteoblasts on a type I atelocollagen grafted ozone oxidized poly L-lactic acid membrane. *Biomaterials* 2001;22:219–30.
- [27] El-Amin SF, Attawia M, Lu HH, Shah AK, Chang R, Hickok NJ, Tuan RS, Laurencin CT. Integrin expression by human osteoblasts cultured on degradable polymeric materials applicable for tissue engineered bone. *J Orthopaed Res* 2002;20:20–8.
- [28] Mikos AG, Sarakinos G, Lyman MD, Ingber DE, Vacanti JP, Langer R. Prevascularization of porous biodegradable polymers. *Biotech Bioeng* 1993;42:716–23.
- [29] Park A, Cima LG. In vitro cell response to differences in poly L-lactide crystallinity. *J Biomed Mater Res* 1996;31:117–30.
- [30] Flemming RG, Murphy CJ, Abrams GA, Goodman SL, Nealey PF. Effects of synthetic micro- and nano-structured surfaces on cell behavior. *Biomaterials* 1999;20:573–88.
- [31] Dalby MJ, Riehle MO, Johnstone JHJ, Affrossman S, Curtis ASG. Polymer-demixed nanotopography: control of fibroblast spreading and proliferation. *Tissue Eng* 2002;8:1099–108.
- [32] Fan YW, Cui FZ, Hou SP, Xu QY, Chen LN, Lee IS. Culture of neural cells on silicon wagers with nano-scale surface topograph. *J Neurosci Methods* 2002;120:17–23.
- [33] Thapa A, Webster TJ, Haberstroh KM. Polymers with nano-dimensional surface features enhance bladder smooth muscle adhesion. *J Biomed Mater Res* 2003;67A:1374–83.
- [34] Sgarbi N, Pisignano D, Di Benedetto F, Gigli G, Cingolani R, Rinaldi R. Self-assembled extracellular matrix protein networks by microcontact printing. *Biomaterials* 2004;25:1349–53.
- [35] Abrams GA, Goodman SL, Nealey PF, Franco M, Murphy CJ. Nanoscale topography of the basement membrane underlying the corneal epithelium of the rhesus macaque. *Cell Tissue Res* 2000;299:39–46.
- [36] Curtis A, Riehle M. Tissue engineering: the biophysical background. *Phys Med Biol* 2001;46:R47–65.
- [37] Ruardy TG, Schakenraad JM, van der Mei HC, Busscher HJ. Adhesion and spreading of human skin fibroblasts on physico-chemically characterized gradient surfaces. *J Biomed Mater Res* 1995;29:1415–23.
- [38] Burdick JA, Khademhosseini A, Langer R. Fabrication of gradient hydrogels using a microfluidics/photopolymerization process. *Langmuir* 2004;20:5153–6.
- [39] Kang CE, Gemeinhar JR, Gemeinhart RA. Cellular alignment by grafted adhesion peptide surface density gradients. *J Biomed Mater Res* 2004;71A:403–11.
- [40] Li B, Ma Y, Wang S, Moran PM. A technique for preparing protein gradients on polymeric surfaces: effects on PC12 pheochromocytoma cells. *Biomaterials* 2004;26:1487–95.
- [41] Smith JT, Tomfohr JK, Wells MC, Beebe Jr TP, Kepler TB, Reichert WM. Measurement of cell migration on surface-bound fibronectin gradients. *Langmuir* 2004;20:8279–86.
- [42] Brocchini S, James K, Tangpasuthadol V, Kohn J. Structure-property correlations in a combinatorial library of degradable biomaterials. *J Biomed Mater Res* 1998;42:66–75.
- [43] Anderson DG, Levenberg S, Langer R. Nanoliter-scale synthesis of arrayed biomaterials and application to human embryonic stem cells. *Nature Biotech* 2004;22:863–6.
- [44] Weber N, Bolikal D, Bourke SL, Kohn J. Small changes in the polymer structure influence the adsorption behavior of fibrinogen on polymer surfaces: validation of a new rapid screening technique. *J Biomed Mater Res* 2004;68A:496–503.
- [45] Zhao J-C, Jackson MR, Peluso LA, Brewer LN. A diffusion-multiple approach for mapping phase diagrams, hardness, and elastic modulus. *JOM* 2002;54:42–5.
- [46] Potyrailo RA, Wroczynski RJ, Pickett JE, Rubinsztajn M. High-throughput fabrication, performance testing and characterization of one dimensional libraries of polymeric compositions. *Macromol Rapid Commun* 2003;24:123–30.
- [47] de Gans B-J, Schubert US. Inkjet printing of polymer micro-arrays and libraries: instrumentation, requirements and perspectives. *Macromol Rapid Commun* 2003;24:659–66.
- [48] Cabral JT, Karim A. Discrete combinatorial investigation of polymer mixture phase boundaries. *Meas Sci Technol* 2004;15:1–8.